

An Excess of Globular Clusters in UDGs Formed Through Tidal Heating

Timothy Carleton,^{1*} Yicheng Guo¹, Ferah Munshi², Michael Tremmel³, Anna Wright⁴

¹*Department of Physics and Astronomy, 223 Physics Building, University of Missouri, Columbia, MO 65211, USA*

²*Department of Physics & Astronomy, University of Oklahoma, 440 W. Brooks St., Norman, OK 73019, USA*

³*Yale Center for Astronomy & Astrophysics, Physics Department, P.O. Box 208120, New Haven, CT 06520, USA*

⁴*Department of Physics & Astronomy, Rutgers, The State University of New Jersey, 136 Frelinghuysen Road, Piscataway, NJ 08854, USA*

22 December 2024

ABSTRACT

To investigate the origin of elevated globular cluster abundances observed around Ultra-Diffuse Galaxies (UDGs), we simulate globular cluster populations hosted by UDGs formed through tidal heating. Specifically, globular cluster (GC) formation is modeled as occurring in regions of dense star formation. Because star-formation-rate-densities are higher at high redshift, dwarf galaxies in massive galaxy clusters, which formed most of their stars at high redshift, form a large fraction of their stars in globular clusters. Given that UDGs formed through environmental processes are more likely to be accreted at high redshift, these systems have more GCs than non-UDGs. In particular, our model predicts that massive UDGs have twice the GC mass of non-UDGs of similar stellar mass, in rough agreement with observations. Although this effect is somewhat diminished by GC disruption, we find that the relationship between GC mass fraction and cluster-centric distance, and the relationship between GC mass fraction and galaxy half-light radius are remarkably similar to observations. Among our model objects, both UDGs and non-UDGs present a correlation between halo mass and GC mass, although UDGs have lower dynamical masses at a given GC mass. Furthermore, because of the effectiveness of GC disruption, we predict that GCs around UDGs should have a more top heavy mass function than GCs around non-UDGs. This analysis suggests that dwarfs with older stellar populations, such as UDGs, should have higher globular cluster mass fractions than objects with young stellar populations, such as isolated dwarfs.

Key words: galaxies: formation, evolution, dwarf, haloes, clusters, star clusters

1 INTRODUCTION

The recent identification of a large population of Ultra-Diffuse Galaxies (UDGs) in clusters (van Dokkum et al. 2015) has generated significant interest in Low-Surface-Brightness Galaxies. These dwarf galaxies are characterized by stellar masses ranging from $10^7 - 10^9 M_\odot$ and half-light radii extending from 1.5 to 7 kpc (Koda et al. 2015; Yagi et al. 2016). Observations indicate that, although a population of UDGs is present in low-mass groups and the field (Román & Trujillo 2017a; Leisman et al. 2017), most UDGs are found in cluster environments (van der Burg et al. 2017), and, like other dwarfs in clusters, are characterized by old stellar populations and low metallicities (Ferre-Mateu et al. 2018).

Generally, theories for UDG formation describe them as dwarf galaxies that have been enlarged due to internal or external processes. For example, Amorisco & Loeb (2016) suggested that UDGs represent galaxies living in halos in the high-spin tail of the

spin distribution, with their large sizes the result of high angular-momentum gas. Alternatively, strong feedback from supernovae and stellar winds has been shown to increase the sizes of dwarf galaxies in simulations to resemble UDGs (Di Cintio et al. 2017; Chan et al. 2018). In a similar vein, it has been suggested that the period of globular cluster formation early in the Universe was violent enough in some systems to completely eject their gas, leaving a galaxy with a low stellar mass and large size, but a large halo mass and GC population (Agertz & Kravtsov 2016; van Dokkum et al. 2016). While these models presume that UDGs in clusters have early infall times to prevent re-accretion of gas, other models suggest a more explicit environmental mechanism. For example, ram-pressure stripping or tidal heating may puff up galaxies (Yozin & Bekki 2015; Safarzadeh & Scannapieco 2017; Ogiya 2018). In particular, Carleton et al. (2019) modeled UDGs as tidally-heated dwarfs in clusters, and was able to reproduce many observed UDG properties, such as their size distribution and old stellar populations. Lastly, some comprehensive simulations suggest that a com-

* e-mail: carletont@missouri.edu

bination of these effects may be at play (Jiang et al. 2019; Tremmel et al. 2019; Liao et al. 2019; Sales et al. 2020; Wright et al. 2020).

Observations indicate that the environments in which UDGs are found have a substantial impact on their formation and evolution. The relative abundance of UDGs in a cluster is dependent on the halo mass of the cluster (van der Burg et al. 2017), and the morphologies of UDGs appear to evolve from disks in the field to elongated spheroids in clusters (Burkert 2017; Rong et al. 2019). Furthermore, although a population of UDGs is observed in the field (Williams et al. 2016; Leisman et al. 2017; Román & Trujillo 2017b), they have different properties than UDGs observed in clusters (Prole et al. 2019b), so they may have a distinct formation process than cluster UDGs. However, environmental processes have generally been unable to explain one of the most intriguing aspects of UDGs: their unusual globular cluster (GC) populations. Multiple studies (van Dokkum et al. 2017; Lim et al. 2018; Amorisco et al. 2018; Prole et al. 2019a) have confirmed that a substantial number of UDGs in clusters host exceptionally large GC populations, with > 2 times higher GC abundances than non-UDG dwarfs at a similar stellar mass. Further evidence of the unusual GC populations hosted by UDGs comes from van Dokkum et al. (2018), which found that GCs around the UDG DF2 have an unusually top-heavy luminosity function. However, some observations indicate that UDGs in less dense environments don't show the same elevated GC abundances as UDGs in clusters (Somalwar et al. 2020), suggesting that the cluster environment plays a role in evolution of their GC populations. All of this evidence, along with the unusually high velocity dispersions observed in some UDGs (van Dokkum et al. 2016), has led some to speculate that UDGs in clusters live in over-massive dark-matter halos.

Despite their use as probes of dark-matter halos, there remains significant uncertainty regarding how globular clusters are formed. Their old ages and low metallicities suggest that they primarily form at very high redshift ($z > 5$; Forbes & Bridges 2010; Boylan-Kolchin 2017). On the other hand, the mixed stellar populations of some globular clusters (Gratton et al. 2012), as well as the continued formation of star clusters suggests that globular clusters can be formed and destroyed throughout cosmic time. In particular, the regions of dense star formation at $z = 1 - 2$ (Guo et al. 2015; Elmegreen 2018) may be the progenitors of some of today's globular clusters (Kruijssen 2015).

Notably, observations suggest that the fraction of stars within a gas cloud that form bound clusters (otherwise known as the cluster formation efficiency, Γ) is proportional to the star-formation rate surface density of the gas (Goddard et al. 2010). Previous work has recognized that a consequence of this correlation is that dwarf galaxies that fall into a cluster early (and form most of their stars in high star-formation rate density regions at high z) may be expected to have larger globular cluster populations (Mistani et al. 2016). If UDGs were formed at earlier times than typical dwarf galaxies (as expected by environmental formation models like Carleton et al. 2019, Yozin & Bekki 2015, or Tremmel et al. 2019 and confirmed by observations from Ferre-Mateu et al. 2018 and Ruiz-Lara et al. 2018), it is very likely they formed a higher fraction of their stellar mass in clusters. This offers the possibility that the large globular cluster populations observed in UDGs are a consequence of their early formation. Importantly, this scenario is possible for any model in which UDGs are formed at earlier times than non-UDGs and globular clusters are formed more efficiently at high z .

In this paper, we elaborate on the model of Carleton et al. (2019) to explore the formation of globular clusters in UDGs formed through tidal heating. In particular, we explore the possi-

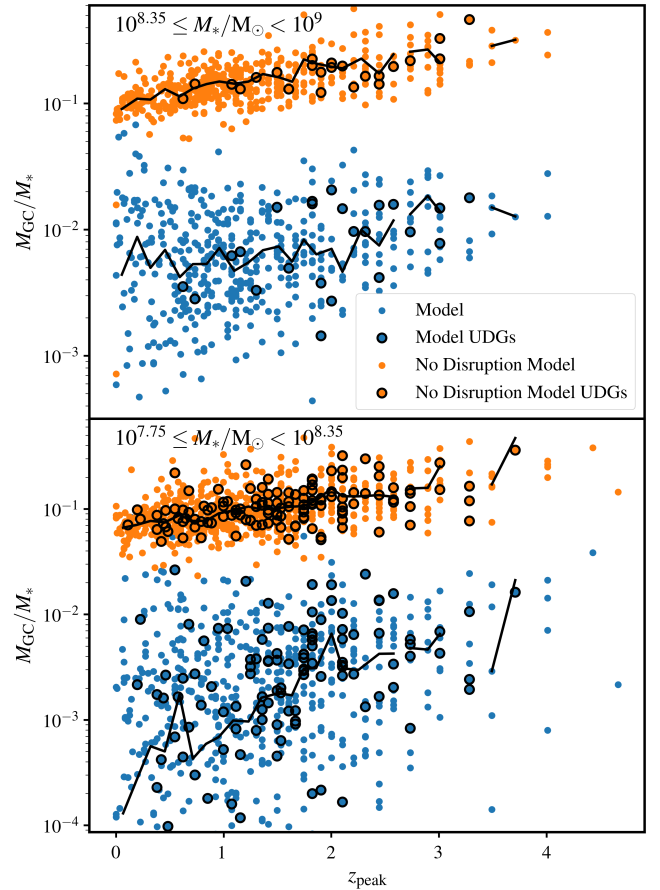


Figure 1. The relationship between GC mass fraction and infall redshift for objects in our model, split into two bins of stellar mass. Our fiducial model is shown as blue points, whereas a model with no GC disruption is shown with orange points. Points outlined in black highlight objects identified as UDGs. Because star formation is more dense at higher redshift, there is a positive correlation between GC fraction and infall redshift in both models: the black lines show the median-binned trend for both samples. Adding disruption substantially increases the scatter in this relationship, but results in more realistic GC fractions.

bility that UDGs have large GC populations because they formed their stellar mass earlier than non-UDGs. In Section 2 we describe our model of UDG formation and their associated GCs. In Section 3 we describe how the GC populations of UDGs and non-UDGs compare, and how they compare with observations. In Section 4 we discuss the limitations of our model when considering low-mass galaxies, and in Section 5 we summarize our conclusions. Throughout, we assume a Λ CDM cosmology based on the Planck Collaboration et al. (2016) cosmological parameters: $H_0 = 67.74 \text{ km s}^{-1} \text{ Mpc}^{-1}$, $\Omega_m = 0.3089$, and $\Omega_\Lambda = 0.6911$.

2 MODEL

To investigate the formation of GCs around cluster UDGs produced through tidal heating, we apply the model for tidal stripping described in Carleton et al. (2019) to the Illustris TNG-100 simulation (Springel et al. 2018; Naiman et al. 2018; Marinacci et al. 2018; Pillepich et al. 2018; Nelson et al. 2018). From the Illustris-TNG Simulation, galaxies are selected from within R_{200}

of a massive cluster with $M_{200} > 2 \times 10^{14} M_{\odot}$ at $z = 0$, where $M_{200} = 200\rho_{\text{crit}} \frac{4\pi}{3} R_{200}^3$ and ρ_{crit} is the critical density of the Universe. The orbits of satellites are tracked throughout their time in the cluster. For each satellite in TNG, the infall stellar mass is taken as the stellar mass of the simulated galaxy at the time of the peak halo mass. Each galaxy is assigned a stellar half-light radius (r_e) based on the size-mass relation for red galaxies from [Lange et al. \(2015\)](#), and its halo is modeled with a cored profile, with a concentration assigned following the mass-concentration relation from [Prada et al. \(2012\)](#).¹ At each pericentric passage, the mass within the tidal radius of the subhalo is used as input to tidal tracks of [Peñarrubia et al. \(2010\)](#) to evolve the V_{max} and r_{max} of the subhalo. The mass within r_{max} of the subhalo at $z = 0$ compared with the mass within r_{max} at infall is used as input for the tracks of [Errani et al. \(2018\)](#) to determine the amount of stellar mass loss and the change in r_e . In this work, we assign all galaxies cored dark-matter halos, which are expected to be the hosts of UDGs produced through tidal heating. As in [Carleton et al. \(2019\)](#), we alter the central slope of the dark-matter halo in baryon-dominated galaxies where the stellar mass within the half-light radius is higher than the dark-matter mass within the half-light radius. This procedure has been able to reproduce many aspects of the UDG population, including the size distribution and the old ages of UDGs.

By analyzing the Illustris-TNG simulation with this procedure, we have access to the cold gas and star-formation-rate properties of dwarf galaxies before and during infall, which can be used to model their globular cluster populations. To generate model globular-cluster populations among our model dwarf galaxies, we reference the procedure of [Mistani et al. \(2016\)](#). This model is based on the observation that the fraction of stars formed in clusters is proportional to the surface density of star formation. From each snapshot of each dwarf galaxy considered, we identify the average surface density of star formation of each gas particle in the dwarfs in our sample as $\Sigma_{\text{SFR}} = \frac{\text{SFR}_3}{\pi r_3^2}$, where SFR_3 is sum of the star formation rates of the 3 nearest star forming gas particles, and r_3 is the distance to the third nearest star-forming gas particle. Following [Goddard et al. \(2010\)](#), we take the fraction of stars formed in clusters (Γ) to be

$$\Gamma = 0.29 \left(\frac{\Sigma_{\text{SFR}}}{M_{\odot} \text{ yr}^{-1} \text{ kpc}^{-2}} \right)^{0.24}. \quad (1)$$

The total globular cluster mass is correspondingly increased by $\Gamma \text{SFR} \Delta t$, where Δt is the time between timesteps in the simulation and SFR is the total star formation rate of the galaxy. Given the mass formed in globular clusters, we populate the globular cluster mass function of [Jordán et al. \(2007\)](#). Each globular cluster is also assigned a position within its host galaxy following a [Plummer \(1911\)](#) distribution with a scale radius 1.5 times the half-light radius of the galaxy. This assumed distribution is motivated by observations indicating that the extent of the GC population around UDGs is similar to the stellar extent ([Amorisco et al. 2018](#)).

While fully accounting for the disruption of globular clusters requires a more precise model for the birth of globular clusters and a higher resolution simulation, we model the effects of dis-

ruption on the globular cluster population to generate a more realistic GC population. Constraints from the distribution of GC ages and masses suggests two primary phases of globular cluster disruption ([Fall & Chandar 2012](#)). First, while the cluster still resides in the disk, interactions with nearby molecular clouds are able to disrupt clusters at a roughly constant rate. Second, once the cluster is outside the disk, tidal interactions with the galaxy disk as well as multi-body interactions within the cluster cause the cluster to evaporate.

To account for tidal disruption of GCs and cluster evaporation, we adopt equations 3 and 4 from [Gnedin et al. \(2014\)](#), using the combined stellar mass and dark-matter profiles to determine the orbital frequency. Each globular cluster is assumed to reside at its birth position for the duration of the simulation.² The rate of disruption due to interactions with gas and stars in the disk (molecular clouds in particular) is less well constrained, particularly for galaxies with low stellar masses, although it has been shown to be related to the density of gas in the disk ([Kruijssen 2015](#)). Rather than fully model the destruction of globular cluster in this phase, we parameterize the disruption rate as a linear function of the stellar and gas mass of the galaxy. In agreement with previous models (e.g. [Kruijssen 2015](#)), we model the GC disruption rate as:

$$\frac{dM(t)}{dt} = M(t)/t_{\text{d, disk}}, \quad (2)$$

where $M(t)$ is the globular cluster mass at simulation time t , and $t_{\text{d, disk}}$ is the disruption timescale due to the fact that the cluster is born in the disk. We parameterize $t_{\text{d, disk}}$ as a function of the stellar mass and gas fraction of the galaxy in the simulation as:

$$\log t_{\text{d, disk}} = C_1 \log \left(\frac{M_{\text{gas}}}{M_*} \right) + C_2 \log \left(\frac{M_*}{M_{\odot}} \right) + C_3, \quad (3)$$

where M_{gas} is the gas mass of the object, and M_* is the stellar mass of the object. The constants C_1 , C_2 , and C_3 are determined to be the best fit values to reproduce the observed ratio of GC-to-stellar mass for three bins of M_* from $10^8 M_{\odot}$ to $10^9 M_{\odot}$. The best fit values are $C_1 = -0.4$, $C_2 = 0$, and $C_3 = 0.33$.

Additionally, we model the effects of tidal stripping of GCs by the cluster environment. To incorporate this effect into our model, we make the assumption that the amount of GC mass stripped is equivalent to the amount of stellar mass stripped:

$$M_{\text{GC, stripped}}/M_{\text{GC, infall}} = M_{*, \text{stripped}}/M_{*, \text{infall}}, \quad (4)$$

where $M_{*, \text{stripped}}/M_{*, \text{infall}}$ is taken from the same [Errani et al. \(2018\)](#) tracks used to model the stellar mass stripping of the galaxy. This is motivated by observations indicating that the extent of globular cluster populations around UDGs are similar to the extent of the stellar disk ([Amorisco et al. 2018](#)). To test the impact of this assumption on our analysis, we run an alternative model using star particles in the simulation as tracer particles (in a method similar to [Mistani et al. 2016](#)). For each GC that is born, we tag a random star particle as representing that GC at its birth. If the star particle is not bound to the galaxy at $z = 0$, the GC is considered to be stripped. This procedure only changes the fraction of stripped GCs by $< 10\%$ (with our fiducial model stripping 10% more GCs than the alternative model), so we conclude that the assumptions of our

¹ Although stellar sizes and halo concentrations are available for individual objects in the simulation, we use model parameters in order to focus specifically on UDGs produced through tidal heating as in the [Carleton et al. \(2019\)](#) model. The comparatively large number of galaxies in the simulation would result in a large number of UDGs produced through internal processes, which are not the focus of this work.

² Within the central cores of the dark-matter halos (where nearly all GCs live), the GC disruption rate is not dependent on galacto-centric radius, so including the effects of dynamical friction would not significantly affect our results.

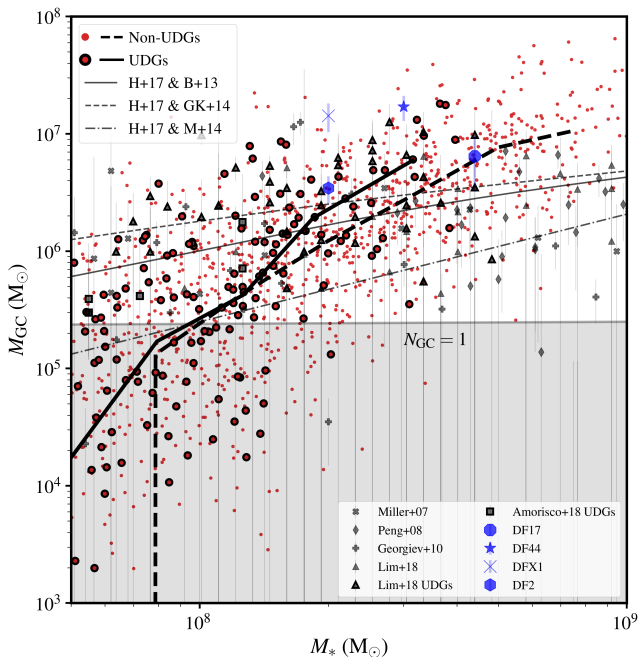


Figure 2. The relationship between stellar mass and globular cluster mass. Circular points are from our model, with systems classified as UDGs highlighted with black outlines. The black dashed and solid lines show the median-binned trend for non-UDGs and UDGs respectively. Grey squares and triangles with black outlines show observations of GCs in UDGs from Amorisco et al. (2018) and Lim et al. (2018), assuming an average mass of $2.3 \times 10^5 M_\odot$ (Harris et al. 2017). Grey “x”s, diamonds, crosses, and triangles are non-UDG observations from Miller & Lotz (2007), Peng et al. (2008), Georgiev et al. (2010), and Lim et al. (2018). The blue octagon, pentagon, star, “X”, and hexagon highlight five notable UDGs of DF17, VCC 1287, DF44, DFX1, and DF2 respectively, from Peng & Lim (2016), Beasley et al. (2016), van Dokkum et al. (2016), van Dokkum et al. (2017) and van Dokkum et al. (2018). The grey lines represent the expectations from a constant M_{GC} -to- M_{halo} ratio of 2.9×10^{-5} (Harris et al. 2017), following the abundance-matching relations of Behroozi et al. 2013 (solid grey line) Garrison-Kimmel et al. 2014 (dashed grey line) and Miller et al. 2014 (dot-dashed line). The grey shaded region highlights where M_{GC} is less than the average mass of one GC from (Harris et al. 2015).

stripping model don’t significantly change our conclusions. Furthermore, tidal stripping by the cluster is a significantly weaker effect than GC disruption in our model, so if the GC population is taken to be significantly more extended, the GC mass actually increases because of the less effective GC disruption. Lastly, we note that while increasing the extent of the GC population weakens the trend between total GC mass and infall time (resulting in a smaller difference between UDGs and non-UDGs), it also weakens the trend between GC abundance and environment (in contrast with existing observations implying a significant environmental dependence to GC abundances, e.g. Peng et al. 2008).

Following this procedure, our analysis generates a population of galaxies affected by tidal heating and stripping, as well as their globular-cluster populations. Figure 1 shows the relationship between the total GC mass-to-stellar mass (M_{GC} -to- M_*) ratio and infall redshift (throughout this analysis, we will focus primarily on the total GC mass formed in our model systems because that is less sensitive to the uncertain nature of GC disruption than the abundance of GCs). This figure also shows how models without dis-

ruption produce GC-to-stellar mass ratios of 10 – 50%, far beyond what is observed.

In agreement with Mistani et al. (2016), we find a strong correlation between GC fraction and infall time. Although this effect is dampened by stripping and disruption of globular clusters, this correlation persists, particularly for systems with infall redshift above 2. On average, we find $\log(M_{GC}/M_*) \propto (0.1 \pm 0.02)z_{inf}$ for massive systems and $\log(M_{GC}/M_*) \propto (0.22 \pm 0.03)z_{inf}$ for less massive systems. Figure 2 compares our models and observations in the $M_{GC} - M_*$ plane. Our model systems approximately line up with observations for objects $M_* \geq 10^{7.75} M_\odot$. While limitations in our modeling (see Sec. 4) prevent an exact match between observations and model points, our models capture the general trend of globular clusters that are continually formed in regions of intense star formation and disrupted. Furthermore, it is clear that UDGs (which have earlier infall times than non-UDGs – see Fig. 1) have significantly higher globular cluster masses than non-UDGs of similar stellar mass.

3 COMPARING GC POPULATIONS OF UDGs AND NON-UDGs

A key prediction of the Carleton et al. (2019) model is that systems with the earliest infall times are most likely to evolve into cluster UDGs (given the greater accumulated tidal effects). As such, objects identified as UDGs (defined as systems with stellar surface density $\Sigma_* = M_*/(\pi r_e^2)$ between 1.73×10^6 and $17.3 \times 10^6 M_\odot \text{ kpc}^{-2}$ and r_e between 1.5 and 7 kpc) tend to have higher M_{GC} values than non-UDG dwarfs at a similar mass. To highlight this difference in particular, we compare the GC mass fraction (M_{GC}/M_*) distributions of UDGs and a stellar mass-matched sample of non-UDG dwarf galaxies in Figure 3. We find that UDGs have a 0.32 dex higher GC fraction than non-UDGs among the most massive systems (right panel). The main cause of this difference in GC populations is the offset infall time distributions between UDGs and non-UDGs. Any model in which UDGs have significantly earlier infall times than non-UDGs (e.g. Yozin & Bekki 2015; Tremmel et al. 2019) should produce an elevated number of GCs in UDGs compared with non-UDGs. A smaller difference between UDGs and non-UDGs is predicted in less massive systems (left panel). This difference is not caused by the slight difference between GC formation and disruption among high- and low-mass dwarfs (in fact, because disruption is more efficient in high-mass dwarfs, there is a stronger correlation between GC fraction and infall time for low-mass dwarfs than high-mass dwarfs); rather, a larger fraction of low-mass UDGs have later infall times (Fig. 1). This is because lower mass dwarfs only require $\sim 50\%$ expansion to be considered a UDG, whereas higher mass dwarfs must expand by a factor of ~ 2 based on our assumed mass-size relation. If galaxies are larger at infall (as suggested by simulations: e.g. Genel et al. 2018; Tremmel et al. 2019; Jiang et al. 2019; Wright et al. 2020) less expansion is required, so the difference in GC populations may be less significant.

To further compare our model with observations, Figure 4 shows the relationship between globular cluster mass fraction and galaxy half-light radius for objects with $M_* \geq 10^{8.35} M_\odot$. As both tidal expansion and globular cluster mass fraction are correlated with infall time, our model predicts a positive correlation between GC fraction and size among UDGs and non-UDGs (Spearman rank correlation p value is 0.008). Among model points with $M_{GC} > 0$, we find $\log(M_{GC}/M_*) \propto (0.5 \pm 0.2) \log(r_e)$, which is very simi-

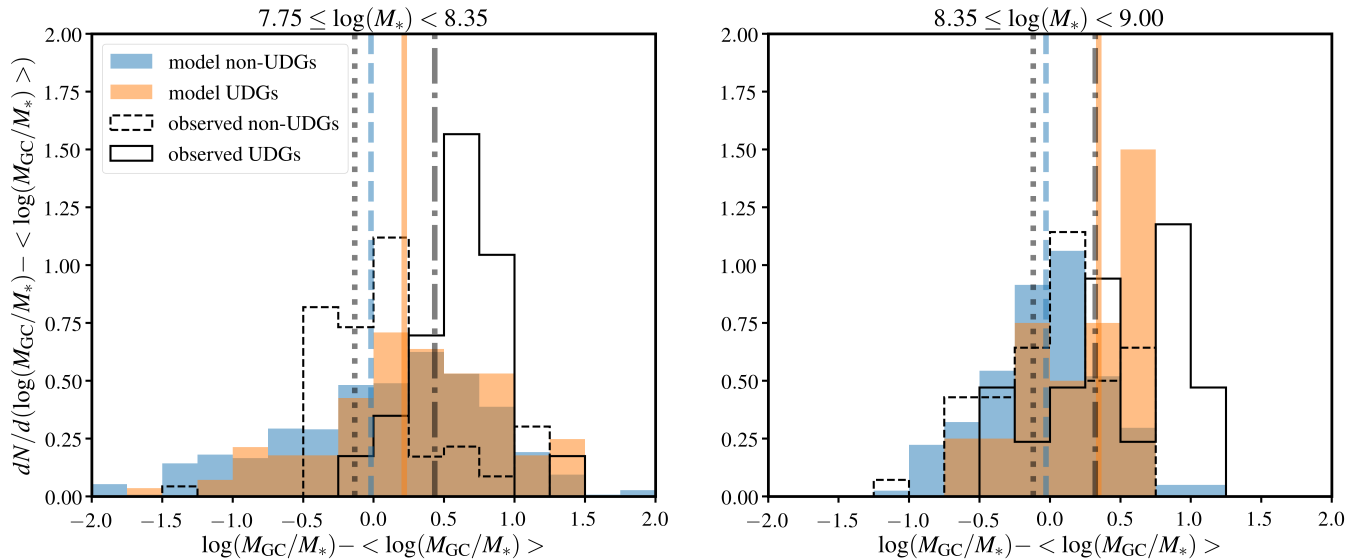


Figure 3. A comparison of the globular cluster populations of UDGs and non-UDGs among less massive ($10^{7.75} \leq M_*/M_\odot < 10^{8.35}$; left) and more massive ($10^{8.35} \leq M_*/M_\odot < 10^9$; right) objects. The blue and orange solid histograms show the GC mass fraction distributions from our model for a mass-matched sample of non-UDGs and UDGs respectively. To facilitate a comparison with observations, we have offset the distributions by the median GC mass fraction of all simulated objects in the appropriate mass range. Solid and dashed black histograms illustrate the mass-matched distributions for observed UDGs and non-UDGs from [Miller & Lotz \(2007\)](#), [Peng et al. \(2008\)](#), [Georgiev et al. \(2010\)](#), [Beasley et al. \(2016\)](#), [van Dokkum et al. \(2016\)](#), [van Dokkum et al. \(2017\)](#), [Lim et al. \(2018\)](#), and [van Dokkum et al. \(2018\)](#) offset by the median *observed* GC mass fraction for this sample. The solid orange and black lines show the median values for simulated and observed UDGs respectively, whereas the dashed blue and dotted black lines show the median values for non-UDGs. Our model predicts that massive UDGs have a 0.32 dex higher GC mass fraction than non-UDGs, similar to observations finding an offset of 0.20 dex. Less massive UDGs have a 0.18 dex higher GC mass fraction than non-UDGs, compared with observations finding a 0.49 dex offset.

lar to observations showing $\log(M_{GC}/M_*) \propto (0.6 \pm 0.2) \log(r_e)$. That this correlation persists for all r_e values highlights the fact that UDGs are not unique in this model, but simply the high-size tail of the galaxy population. Similarly, Figure 5 shows the correlation between GC fraction and cluster-centric distance. A slight negative correlation between globular cluster fraction and cluster-centric distance is present, again resulting from the correlations between infall time, cluster-centric distance, and GC fraction. This trend is consistent between UDGs and non-UDGs and is similar to the trend observed among non-UDGs in Virgo ([Peng et al. 2008](#)). Observations of UDGs have not yet been able to probe a large range of cluster-centric distances, but our predicted trend is consistent with a slight negative correlation between GC mass fraction and cluster-centric distance among existing observations of UDGs ([Lim et al. 2018](#)). We predict that a similar trend will be present among UDGs and non-UDGs once objects in the cluster outskirts can be studied in more detail. Specifically, we find $\log(M_{GC}/M_*) \propto (-0.30 \pm 0.06) \log(D_{\text{host}}/R_{200})$.

Given the constant ratio of GC mass-to-dark-matter mass ratio observed among massive objects ([Harris et al. 2017](#)), GC populations have been particularly intriguing as a window to the dark-matter mass of galaxies. In Figure 6, we plot globular cluster mass vs. both total halo mass (left) and dynamical mass as probed by stellar velocity dispersion (right). Stellar velocity dispersions are determined using the line-of-sight Virial Theorem assuming a Plummer stellar distribution and the stripped dark-matter density profile, as in [Carleton et al. \(2019\)](#). Notably, our model is within 0.1 dex of the M_{GC}/M_{halo} ratio observed in massive galaxies ([Harris et al. 2017](#)) for objects with $M_{\text{halo}} > 10^{10} M_\odot$, despite our use of observations of the M_{GC}/M_* ratio, not the M_{GC}/M_{halo} ratio, to constrain our model. However, a large degree (~ 1 dex) of scatter is present,

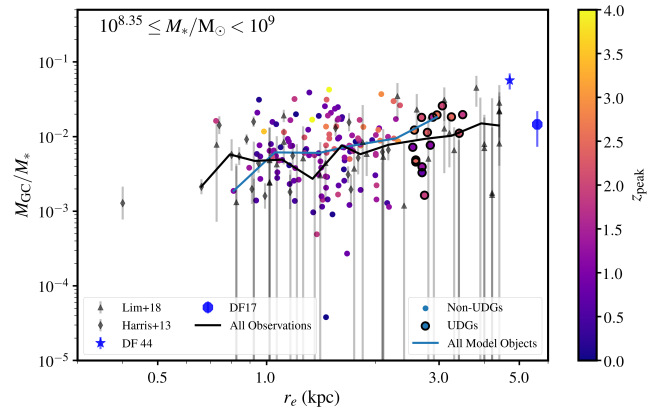


Figure 4. The relationship between GC mass fraction and size among a mass-matched sample of UDG and non-UDG model systems with $M_* \geq 10^{8.35} M_\odot$, as well as observed systems. Circular points are from our model, color-coded by z_{peak} (the redshift of the objects maximum halo mass), and systems classified as UDGs are highlighted with black outlines. Grey triangles are observations from [Lim et al. \(2018\)](#) and grey diamonds are from the [Harris et al. \(2013\)](#) collection of observations. As in Fig. 2, the blue star refers to DF44 ([van Dokkum et al. 2016](#)) and the blue octagon refers to DF17 ([Peng & Lim 2016](#)). The blue line shows the median GC fraction among all model objects (UDGs and non-UDGs) in bins of r_e , and the black line shows the binned median points considering all observations. Model objects show a positive trend between size and GC fraction, both of which are correlated with infall redshift. This is consistent with the strong trend observed between size and globular cluster fraction in massive dwarf galaxies.

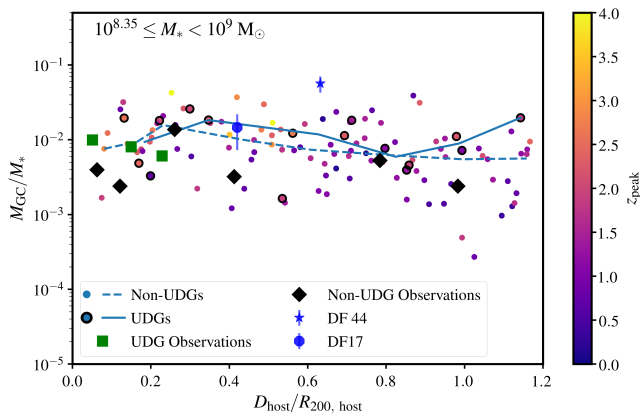


Figure 5. The relationship between globular cluster fraction and cluster-centric distance (normalized to R_{200} of the host cluster). The relative frequency of globular clusters increases as systems approach the cluster center because early infalling dwarfs with larger globular cluster populations are able to sink toward the cluster center. The model symbols are the same as in Fig. 4. Observations of a large number of systems in the cluster outskirts are difficult to obtain, but we show the binned median GC fraction for observed UDGs (green squares) and non-UDGs (black diamonds). Future observations of GCs around UDGs in the cluster outskirts can further test the predicted environmental dependence of GC mass among UDGs.

compared with the 0.26 dex scatter seen observationally (Harris et al. 2017). Additionally, UDGs have systematically lower globular cluster masses at a given halo mass (by 0.4 dex; left panel) and dynamical mass (by 0.8 dex; right panel). There are two reasons for the offsets between UDGs and non-UDGs in this space. Firstly, UDGs with the largest halo masses are selected to have the latest infall times (because they are relatively unaffected by stripping), and thus lower GC masses (Fig. 1). Secondly, the tidal heating process increases an object’s dynamical mass: as the stellar extent of a system increases substantially, dark-matter is preferentially stripped from the halo outskirts, leaving the central region probed by the stellar velocity dispersion largely intact. This results in higher dynamical masses for UDGs compared with non-UDGs (Carleton et al. 2019; Errani et al. 2018). This prediction is in marginal conflict with a small number of observations indicating that UDGs and non-UDGs have a similar GC mass for a given dynamical mass. Future observations with large samples of UDGs are needed to explore the full range of dynamical masses for a given GC mass. While this suggests that GC abundances may be better at estimating total halo mass than stellar dynamics, our modeling relies on more assumptions (a constant cluster formation fraction, a constant GC initial mass function, a constant GC radial distribution, and an unevolving dwarf-elliptical size-mass relation) than dynamical probes, and our models have difficulty in reproducing the GC populations of lower mass dwarfs. Nevertheless, this result *does* show that a constant GC-to-halo mass ratio does not necessarily preclude a continuous GC formation process. An important caveat to this result is that a significant correlation between GC-to-halo mass ratio and infall redshift is present that could systematically affect halo mass inferences from GC abundances. Lastly, we note that the presence of systems like DF44, with a high GC mass for its dynamical mass, suggests that some UDGs may have a different formation path.

A specific consequence of this model is a correlation between satellite infall time and globular cluster abundance (Fig. 1). Obser-

vationally, this manifests as a trend between GC fraction and stellar age (characterized by t_{90} : the lookback time at which a galaxy’s stellar mass first reaches 90% of its peak stellar mass), which is shown in Fig. 7 for objects in two stellar mass bins. Although GC stripping and destruction substantially dampen the trend between stellar age and GC mass fraction for massive objects and objects with younger ages, a correlation between GC mass fraction and stellar age is present among less massive objects that should be detectable in future observations. Among objects with t_{90} greater than 7 Gyr and $M_{GC} > 0$, we find $\log(M_{GC}/M_*) \propto (1.1 \pm 0.7) \log(t_{90}/\text{Gyr})$ for objects with $M_* \geq 10^{8.35} M_\odot$ (Fig. 7 upper panel) and $\log(M_{GC}/M_*) \propto (3.3 \pm 0.3) \log(t_{90}/\text{Gyr})$ for objects with $10^{7.75} \leq M_* < 10^{8.35} M_\odot$ (Fig. 7 lower panel). Again, this trend is roughly the same between UDGs and non-UDGs; however, there is a ~ 0.5 dex offset among the oldest systems. This offset is because of systems affected by early pre-processing (note objects with late z_{peak} values but early t_{90} values in Fig. 7). In our model, systems that fall into a group at high z have lower GC formation rates after falling into the group because of the decreased SFR densities. However, some gas is still present in the disk, so GCs are still disrupted at a rapid rate, resulting in lower GC masses at $z = 0$.

Another observable consequence of this model is that objects with early infall times have more top-heavy GC mass functions at $z = 0$, as illustrated in the stacked GC mass functions in Fig. 8. This is because the less massive GCs are not able to survive many Gyr without evaporating. Specifically, systems with infall redshifts > 2 have a 0.44 dex higher mean GC mass than systems with later infall times. As UDGs have preferentially early infall times, they have a 0.13 dex higher mean GC mass than non-UDGs. This offset is important to note, particularly as observations typically assume a constant GC luminosity function to correct for incompleteness among observations of lower mass GCs (e.g. Lim et al. 2018). This also illustrates how a UDG like DF2 could have a very top heavy mass function, and should be testable in future observations. Similarly, GCs in early infall systems have older stellar ages than those in later infall systems, but this difference (~ 11 Gyr old vs. ~ 8 Gyr old) may be difficult to distinguish observationally.

4 GCS IN LOW-MASS GALAXIES

Our model predicts that GCs should be very sparse in the lowest mass ($M_* < 10^{7.75} M_\odot$) galaxies. This is in contrast with observations indicating that GCs are present in most systems above $10^7 M_\odot$, pointing to an incompleteness in our model. This discrepancy is magnified because low mass galaxies only have a handful of GCs — a few additional GCs can double the globular cluster abundance among these systems. Illustris-TNG is limited by temporal and spatial resolution at very high redshifts, so primordial GC formation is largely excluded from our analysis. The presence of a small number of primordial GCs in low mass galaxies would be enough to resolve the discrepancy between our model points and observations while preserving our results for higher mass objects. Additionally, assumptions in our modeling of GC disruption in low-mass objects could affect our ability to accurately characterize the GC population around these systems. For example, it is possible that globular clusters in low mass galaxies are able to escape to larger galacto-centric radii (given the weaker gravitational pull of the galaxy), and become less susceptible to disruption. Altogether, while our model is effective for high-mass dwarfs, illustrating the

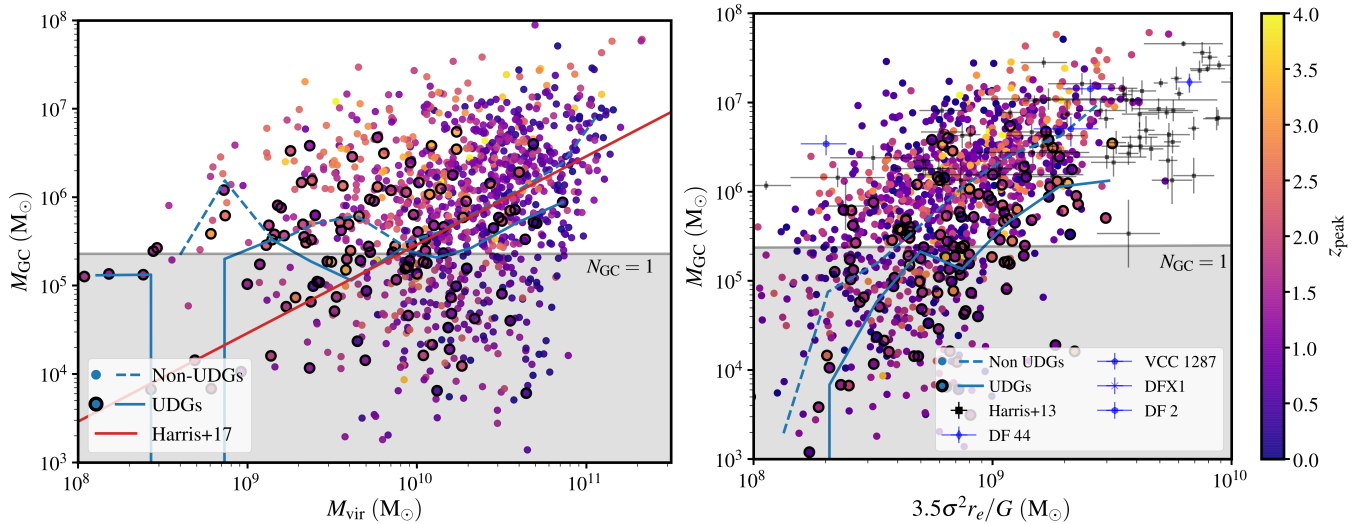


Figure 6. Left: The relationship between GC mass and halo mass for objects with $M_* > 10^{7.75} M_\odot$. Symbols are the same as in Fig. 4, and the red line is the constant GC-to-halo mass ratio from Harris et al. (2017). Non-UDGs in our model reproduce the GC-to-halo mass ratio for massive objects. However, UDGs have a slightly lower GC-to-halo mass ratio. **Right:** The relationship between total globular cluster mass and dynamical mass (as probed by stellar velocity dispersion) for dwarf galaxies. Because UDGs have a higher dynamical mass than non-UDGs of similar stellar mass, there is an offset between UDGs and non-UDGs in this space among our models that may be seen in future observations.

effect of infall time on total GC mass, these limitations prevent an accurate modeling of GCs around low mass dwarfs.

5 CONCLUSION

We combine models for globular cluster and UDG formation to investigate the expected GC populations of tidally-heated UDGs in clusters. Two key features of our model are that GCs are formed more efficiently at high redshift and UDGs have preferentially early infall times. Combined, these features suggest that UDGs in our model have higher GC abundances than non-UDGs of similar mass.

- Observations finding that UDGs have a higher GC mass than non-UDGs can be explained in a scenario in which GCs are formed during periods of intense star formation at high z and UDGs are formed through tidal heating of normal dwarfs with early cluster infall times.
- This model predicts that a galaxy's GC mass fraction should be correlated with its stellar age, half-light radius, and cluster-centric distance.
- This model also predicts that UDGs should have a more top-heavy GC mass function than non-UDGs (in qualitative agreement with one observation), so extrapolating GC abundances based on a non-UDG GC mass function may overestimate the true GC abundance.
- A correlation between the GC-to-halo mass ratio of dwarf galaxies and their infall time is expected, and UDGs are predicted to have lower GC-to-halo mass ratios and lower GC-to-dynamical mass ratios than non-UDGs.

ACKNOWLEDGMENTS

TMC is grateful for Manoj Kaplinghat for his helpful comments. Additionally, the authors are grateful to the anonymous reviewer for their constructive comments. This research made use of *Astropy*,

a community-developed core Python package for Astronomy (Astropy Collaboration et al. 2013). Additionally, the Python packages NumPy (Walt et al. 2011), iPython (Perez & Granger 2007), SciPy (Jones et al. 2001), and matplotlib (Hunter 2007) were utilized for the majority of our data analysis and presentation.

REFERENCES

- Agertz O., Kravtsov A. V., 2016, *ApJ*, **824**, 79
 Amorisco N. C., Loeb A., 2016, *MNRAS*, **459**, L51
 Amorisco N. C., Monachesi A., Agnello A., White S. D. M., 2018, *MNRAS*, **475**, 4235
 Astropy Collaboration et al., 2013, *A&A*, **558**, A33
 Beasley M. A., Romanowsky A. J., Pota V., Navarro I. M., Martinez Delgado D., Neyer F., Deich A. L., 2016, *ApJ*, **819**, L20
 Behroozi P. S., Wechsler R. H., Conroy C., 2013, *ApJ*, **770**, 57
 Boylan-Kolchin M., 2017, *MNRAS*, **472**, 3120
 Burkert A., 2017, *ApJ*, **838**, 93
 Carleton T., Errani R., Cooper M., Kaplinghat M., Peñarrubia J., Guo Y., 2019, *MNRAS*, **485**, 382
 Chan T. K., Kereš D., Wetzel A., Hopkins P. F., Faucher-Giguère C. A., El-Badry K., Garrison-Kimmel S., Boylan-Kolchin M., 2018, *MNRAS*, **478**, 906
 Di Cintio A., Brook C. B., Dutton A. A., Macciò A. V., Obreja A., Dekel A., 2017, *MNRAS*, **466**, L1
 Elmegreen B. G., 2018, *ApJ*, **869**, 119
 Errani R., Peñarrubia J., Walker M. G., 2018, *MNRAS*, **481**, 5073
 Fall S. M., Chandar R., 2012, *ApJ*, **752**, 96
 Ferre-Mateu A., et al., 2018, preprint, ([arXiv:1801.09695](https://arxiv.org/abs/1801.09695))
 Forbes D. A., Bridges T., 2010, *MNRAS*, **404**, 1203
 Garrison-Kimmel S., Boylan-Kolchin M., Bullock J. S., Lee K., 2014, *MNRAS*, **438**, 2578
 Genel S., et al., 2018, *MNRAS*, **474**, 3976
 Georgiev I. Y., Puzia T. H., Goudfrooij P., Hilker M., 2010, *MNRAS*, **406**, 1967
 Gnedin O. Y., Ostriker J. P., Tremaine S., 2014, *ApJ*, **785**, 71
 Goddard Q. E., Bastian N., Kennicutt R. C., 2010, *MNRAS*, **405**, 857
 Gratton R. G., Carretta E., Bragaglia A., 2012, *A&ARv*, **20**, 50

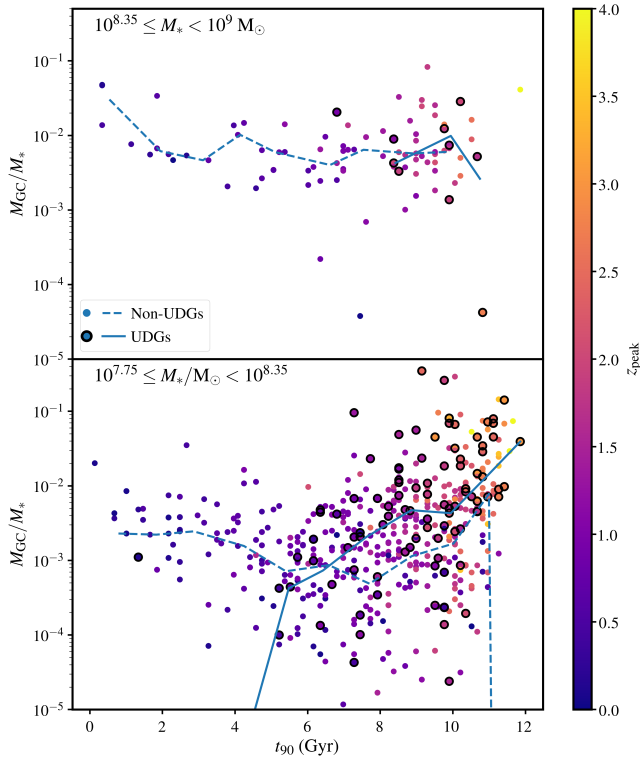


Figure 7. The correlation between GC fraction and stellar age (as defined by the lookback time for which 90% of stars are formed). Both UDGs and non-UDGs with early ($t_{90} > 7$ Gyr) quenching times have significantly higher GC fractions than later infalling systems.

Guo Y., et al., 2015, *ApJ*, **800**, 39
Harris W. E., Harris G. L. H., Alessi M., 2013, *ApJ*, **772**, 82
Harris W. E., Harris G. L., Hudson M. J., 2015, *The Astrophysical Journal*, **806**, 36
Harris W. E., Blakeslee J. P., Harris G. L. H., 2017, *ApJ*, **836**, 67
Hunter J. D., 2007, *Computing in Science & Engineering*, **9**, 90
Jiang F., Dekel A., Freundlich J., Romanowsky A. J., Dutton A. A., Macciò A. V., Di Cintio A., 2019, *MNRAS*, p. 1490
Jones E., Oliphant T., Peterson P., et al., 2001, *SciPy: Open source scientific tools for Python*, <http://www.scipy.org/>
Jordán A., et al., 2007, *ApJS*, **171**, 101
Koda J., Yagi M., Yamanoi H., Komiyama Y., 2015, *ApJ*, **807**, L2
Kruijssen J. M. D., 2015, *MNRAS*, **454**, 1658
Lange R., et al., 2015, *MNRAS*, **447**, 2603
Leisman L., et al., 2017, *ApJ*, **842**, 133
Liao S., et al., 2019, *MNRAS*, **490**, 5182
Lim S., Peng E. W., Côté P., Sales L. V., den Brok M., Blakeslee J. P., Guhathakurta P., 2018, *The Astrophysical Journal*, **862**, 82
Marinacci F., et al., 2018, *MNRAS*, **480**, 5113
Miller B. W., Lotz J. M., 2007, *ApJ*, **670**, 1074
Miller S. H., Ellis R. S., Newman A. B., Benson A., 2014, *ApJ*, **782**, 115
Mistani P. A., et al., 2016, *MNRAS*, **455**, 2323
Naiman J. P., et al., 2018, *MNRAS*, **477**, 1206
Nelson D., et al., 2018, *MNRAS*, **475**, 624
Ogiya G., 2018, *MNRAS*, **480**, L106
Peñarrubia J., Benson A. J., Walker M. G., Gilmore G., McConnachie A. W., Mayer L., 2010, *MNRAS*, **406**, 1290
Peng E. W., Lim S., 2016, *ApJ*, **822**, L31
Peng E. W., et al., 2008, *ApJ*, **681**, 197
Pillepich A., et al., 2018, *MNRAS*, **475**, 648
Planck Collaboration et al., 2016, *A&A*, **594**, A13
Plummer H. C., 1911, *MNRAS*, **71**, 460

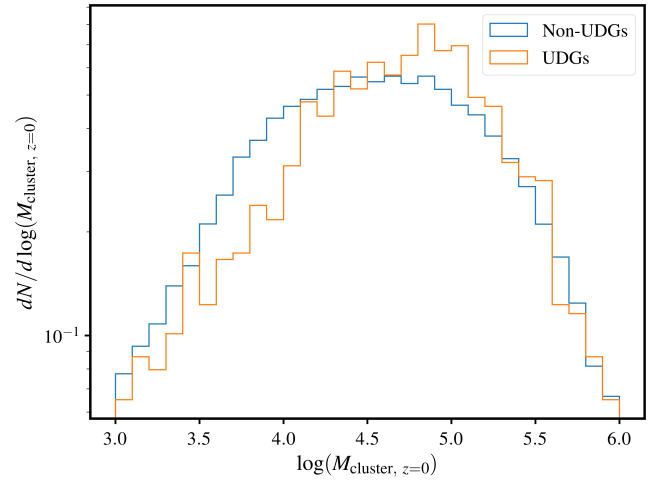


Figure 8. The stacked $z = 0$ GC mass function for both non-UDGs (blue) and UDGs (orange). Because UDGs form their GCs at a higher redshift than non-UDGs, more low-mass GCs are destroyed by disruptive disk and tidal effects, resulting in a more top-heavy GC mass function.

Prada F., Klypin A. A., Cuesta A. J., Betancort-Rijo J. E., Primack J., 2012, *MNRAS*, **423**, 3018
Prole D. J., et al., 2019a, *MNRAS*, **484**, 4865
Prole D. J., van der Burg R. F. J., Hilker M., Davies J. I., 2019b, *MNRAS*, **488**, 2143
Prez F., Granger B. E., 2007, *Computing in Science & Engineering*, **9**, 21
Román J., Trujillo I., 2017a, *MNRAS*, **468**, 4039
Román J., Trujillo I., 2017b, *MNRAS*, **468**, 4039
Rong Y., et al., 2019, *arXiv e-prints*, p. arXiv:1907.10079
Ruiz-Lara T., et al., 2018, *MNRAS*,
Safarzadeh M., Scannapieco E., 2017, *ApJ*, **850**, 99
Sales L. V., Navarro J. F., Peñafiel L., Peng E. W., Lim S., Hernquist L., 2020, *MNRAS*, **494**, 1848
Somalwar J. J., Greene J. E., Greco J. P., Huang S., Beaton R. L., Goulding A. D., Lancaster L., 2020, *arXiv e-prints*, p. arXiv:2008.02806
Springel V., et al., 2018, *MNRAS*, **475**, 676
Tremmel M., Wright A. C., Brooks A. M., Munshi F., Nagai D., Quinn T. R., 2019, *arXiv e-prints*, p. arXiv:1908.05684
Walt S. v. d., Colbert S. C., Varoquaux G., 2011, *Computing in Science & Engineering*, **13**, 22
Williams R. P., et al., 2016, *MNRAS*, **463**, 2746
Wright A. C., Tremmel M., Brooks A. M., Munshi F., Nagai D., Sharma R. S., Quinn T. R., 2020, *arXiv e-prints*, p. arXiv:2005.07634
Yagi M., Koda J., Komiyama Y., Yamanoi H., 2016, *ApJS*, **225**, 11
Yozin C., Bekki K., 2015, *MNRAS*, **452**, 937
van Dokkum P. G., Abraham R., Merritt A., Zhang J., Geha M., Conroy C., 2015, *ApJ*, **798**, L45
van Dokkum P., et al., 2016, *ApJ*, **828**, L6
van Dokkum P., et al., 2017, *ApJ*, **844**, L11
van Dokkum P., et al., 2018, *ApJ*, **856**, L30
van der Burg R. F. J., et al., 2017, *A&A*, **607**, A79